Build Simul (2022) 15: 2097–2110
https://doi.org/10.1007/s12273-022-0917-9

Airborne transmission during short-term events: Direct route over indirect route

Xiujie Li[1], Zhengtao Ai[2,3] (✉), Jinjun Ye[2,3], Cheuk Ming Mak[1], Hai Ming Wong[4]

1. Department of Building Environment and Energy Engineering, The Hong Kong Polytechnic University, Hong Kong, China
2. Department of Civil Engineering, Hunan University, Changsha, China
3. National Center for International Research Collaboration in Building Safety and Environment, Hunan University, Changsha, China
4. Faculty of Dentistry, The University of Hong Kong, Hong Kong, China

Abstract

Numerous short-term exposure events in public spaces were reported during the COVID-19 pandemic, especially during the spread of Delta and Omicron. However, the currently used exposure risk assessment models and mitigation measures are mostly based on the assumption of steady-state and complete-mixing conditions. The present study investigates the dynamics of airborne transmission in short-term events when a steady state is not reached before the end of the events. Large-eddy simulation (LES) is performed to predict the airborne transmission in short-term events, and three representative physical distances between two occupants are examined. Both time-averaged and phase-averaged exposure indices are used to evaluate the exposure risk. The results present that the exposure index in the short-term events constantly varies over time, especially within the first 1/ACH (air changes per hour) hour of exposure between occupants in close proximity, posing high uncertainty to the spatial and temporal evolutions of the risk of cross-infection. The decoupling analysis of the direct and indirect airborne transmission routes indicates that the direct airborne transmission is the predominated route in short-term events. It suggests also that the general dilution ventilation has a relatively limited efficiency in mitigating the risk of direct airborne transmission, but determines largely the occurrence time of the indirect one. Given the randomness, discreteness, localization, and high-risk characteristics of direct airborne transmission, a localized method that has a direct interference on the respiratory flows would be better than dilution ventilation for short-term events, in terms of both efficiency and cost.

Keywords

airborne transmission;
short-term events;
direct exposure;
transient computational fluid dynamics (CFD);
exposure risk

Article History

Received: 16 April 2022
Revised: 06 June 2022
Accepted: 22 June 2022

1 Introduction

The COVID-19 pandemic, caused by the novel SARS-CoV-2 coronavirus, has swept across the world. It has led to 496 million infections including over 6 million deaths as of April 12, 2022 (WHO 2022). Owing to the detection of the positive samples of the SARS-CoV-2 virus RNA in human exhaled particles (Liu et al. 2020), it is of crucial importance in preventing airborne transmission between persons, especially at short physical distances. To a large extent, a lot of concerns have currently been raised about how to prevent the transmission of SARS-CoV-2 variants and achieve economic recovery (Li et al. 2021c).

Three main transmission routes for SARS-CoV-2 have been identified: (indirect) contact, droplet transmission, and airborne transmission. Transmission through contact can be suppressed by strict surface disinfection. When the virus-carrying particles exhaled from an infected subject have settled on the skin or mucous of a susceptible subject, the droplet transmission could occur (Li et al. 2021a). This route of transmission always takes place at a close physical distance. With regard to the airborne transmission, the respiratory micro-droplets (nuclei) suspended in the exhaled air stream could be transmitted to extended distances. The finding of 1 hour half-life of viable SARS-CoV-2 in micro-droplets (Van Doremalen et al. 2020) suggests that the

E-mail: zhengtaoai@hnu.edu.cn

unconscious infection could occur when the virus-charged particles are being inhaled. A series of precautionary measures have been proposed to prevent the probability of contact and droplet transmissions, like keeping a physical distance (such as, larger than 1–2 m), wearing a face mask, and frequent hand washing. Since airborne transmission is relatively more complicated in mechanisms and mitigation measures, the understanding of the airborne transmission routes of SARS-CoV-2 is far from sufficient.

During the COVID-19 pandemic, numerous short-term (unsteady-state) exposure events in public spaces have been reported, and the cross-transmission of the Delta variant of SARS-CoV-2 is reported to occur even in 15 seconds (Kongnov 2021; Times 2021). The clustered outbreaks highlight the importance to evaluate the transient cross-transmission risks of susceptible subjects and then to determine the mitigation and protection measures. However, many past studies focusing on airborne transmission were limited to the steady-state conditions by the two-equation Reynolds-averaged Navier-Stokes (RANS) turbulence models. In computational fluid dynamics (CFD) context, the numerical simulation has been widely employed to study the transmission in different scenarios like the hospitals (Satheesan et al. 2020; Massarotti et al. 2021), office rooms (Wang et al. 2020; Srivastava et al. 2021; Motamedi et al. 2022), vehicles (Zhang et al. 2021; Armand and Tâche 2022; Zhao et al. 2022), and aircraft cabins (Bhatia and De Santis 2020; Desai et al. 2021). The aforementioned limitation of low time-resolution studies posts a need to explore the dynamic process of the transmission of exhaled particles. The process of airborne transmission could be divided into three parts: infected individuals releasing virus-laden aerosols through the exhaled stream, the transportation of aerosols in the air, and the inhalation of aerosols by the susceptible subjects. In order to analyze the dynamics of airborne transmission, it is necessary to decouple the airborne transmission routes, namely the direct and indirect ways and to further analyze separately their characteristics. The oversimplification model with "exhalation only" for the infected subjects cannot reproduce the real situation (Villafruela et al. 2016; Yang et al. 2016; Wu and Weng 2021), since the particles could only be released in the exhalation phase and the breathing flow rate is highly time-dependent. In addition, the airborne cross-transmission is considerably affected by the flow interaction in the breathing zone, including respiratory flow, ventilation flow, and thermal convective boundary layer rising from the heated human body. Overall, the study on the short-term exposure events when steady-state and complete-mixing are not reached before the end of events could provide evidence for the development of precautionary and mitigation measures.

Plenty of the exposure risk assessment models applied to the indoor environment is not suitable for short-term exposure events (Ai and Melikov 2018). For example, the Wells-Riley equations have been widely employed to assess the airborne transmission risk, but the application is based on the assumption of complete mixing and thus it is limited to the steady-state conditions (Riley et al. 1978). However, the contaminant concentration does not rise uniformly in the indoor environment, and there are many unsteady or short-term exposure events in practice when a steady state is not achieved before the end of events, such as physician consultation and short chat. To accurately evaluate the real-time exposure risk of the susceptible subject at one particular moment, it is quite critical to employ a dynamic evaluation method. Ai et al. (2019a) proposed the measurement and evaluation methods for short-term events on the basis of chamber experiments. However, their study is limited to several measurement points, which are not sufficient to reveal the mechanism of airborne transmission during short-term events.

Owing to the time-consuming and resource-demand characteristics of the experimental research, CFD simulations have been widely conducted to investigate the contaminant dispersion in indoor and outdoor environments. The inter-unit transmission (Ai et al. 2013; Ai and Mak 2014), and even transmission between the adjacent buildings (Dai et al. 2018, 2019) have already been studied since the outbreak of SARS. In addition, the influencing factors like ventilation modes, air change rates, physical distancing, mitigation measures, and even the movement of occupants in the indoor environment have also been extensively explored (Melikov et al. 2020; Li et al. 2021b).

The objective of the present study is to analyze in detail the temporal and spatial characteristics of the airborne transmission, especially in the short-term exposure events when the steady-state and complete-mixing conditions are not achieved. By capturing the interaction between the thermal convective boundary layer, the breathing respiratory flow, and ventilation flow, the direct and indirect airborne transmission would be decoupled. In addition, the short-term and steady-state flow conditions, building-up and steady-state background concentration, as well as the exposure risk with short distance and long distance would then be investigated. As a result, a better understanding of airborne transmission in the short-term exposure events could help to develop the dynamic evaluation method for risk assessment and provide the scientific basis for formulating mitigation measures.

2 Mathematical model

2.1 LES turbulence model

The turbulent flow field is composed of vortices in different

scales, which play distinct roles in turbulence development. With large eddy simulation (LES), two types of motion scales would be separated by a spatial filtering operator. Since the large-scale vortices could significantly affect the average flow, having obvious anisotropy, they would be directly resolved. While the small-scale vortices, having approximate isotropy, would be modeled by a so-called sub-grid scale model. After the spatial filter operation, the filtered continuity and momentum equations of the incompressible Navier–Stokes can be obtained.

The Boussinesq's hypothesis (Hinze 1967) is employed to calculate the sub-grid scale stress tensor τ_{ij} by the equation $3\tau_{ij} - \tau_{kk}\delta_{ij} = -6\mu_{SGS}\overline{S}_{ij}$. For the incompressible flow, the term τ_{kk} is zero, and the term μ_{SGS} is modeled by Smagorinsky-Lilly model in the study (Smagorinsky 1963). The μ_{SGS} is calculated by $\mu_{SGS} = \rho L_S^2 \left|\overline{S}\right|$, where $\left|\overline{S}\right| \equiv \sqrt{2\overline{S_{ij}S_{ij}}}$ and L_S refers to the sub-grid mixing length, calculated by L_S = min (kd, $C_sV^{1/3}$). Here, the C_s is the Smagorinsky constant, empirically chosen to be 0.12. The Smagorinsky-Lilly model has been widely employed to study the flow pattern and contaminant transmission in indoor and outdoor environment (Ai and Mak 2015; Dai et al. 2018; Du et al. 2021).

2.2 Risk assessment model

The exposure risk index $\varepsilon_s(t)$, which indicates the relationship between ventilation and infection risk, has been extensively employed for the contaminant exposure risk evaluation in previous studies (Gao and Niu 2007; Melikov and Dzhartov 2013; Liu et al. 2021).

$$\overline{\varepsilon_s(t)} = \frac{\left[\overline{C_{in}(t) - C_{supply}(t)}\right]}{\left[\overline{C_{exhaust}(t) - C_{supply}(t)}\right]} \quad (1)$$

where $C_{supply}(t)$ and $C_{exhaust}(t)$ refer to the contaminant concentration at the ventilation supply and the exhaust, respectively. $C_{in}(t)$ is the inhaled concentration of the susceptible subject, and the overhead bar represents the average in the range of time t. $\overline{\varepsilon_s(t)} > 1$ indicates the worse air quality in the breathing region of the susceptible subjects than in the background or the ventilation exhaust. Considering the delayed characteristics of the term $C_{exhaust}(t)$ and the high volatility of $C_{in}(t)$, an improved evaluation method proposed by Ai et al. (2019a) was adopted to evaluate the dynamic airborne transmission. Compared with the traditional exposure risk index (Eq. (1)), the improved evaluation method makes it possible to evaluate both real-time exposure risk of the susceptible subject at one particular moment and time-averaged exposure risk over a given period, respectively.

$$\varepsilon_d(t) = \frac{C_{in}(t)}{\overline{C_{exhaust\text{-}steady}}} \quad (2)$$

$$\overline{\varepsilon_d(t)} = \frac{\overline{C_{in}(t)}}{\overline{C_{exhaust\text{-}steady}}} \quad (3)$$

where, $\varepsilon_d(t)$ and $\overline{\varepsilon_d(t)}$ refer to the real-time exposure index and the time-averaged exposure index, respectively. $\overline{C_{exhaust\text{-}steady}}$ means the averaged contaminant concentration at ventilation exhaust when reaching steady-state conditions. Phase-averaged exposure index $\overline{\varepsilon_{phase}(t)}$ is calculated from contaminant concentration sampled only in the inhalation phase:

$$\overline{\varepsilon_{phase}(t)} = \frac{\overline{C_{phase}(t)}}{\overline{C_{exhaust\text{-}steady}}} \quad (4)$$

where, $\overline{C_{phase}(t)}$ refers to the arithmetic mean of the concentration during the inhalation phase. The improved evaluation method could not only avoid the delayed building-up of concentration at the ventilation exhaust but also counteract the intervention factors in measuring the term $C_{in}(t)$ by normalization.

3 Model description

3.1 Simulation description

Short-term exposure events could be divided into two types according to the status of the background pollutant concentration: the steady-state condition and the building-up condition (Ai et al. 2019c). The study focused on the last one, which refers to the infected subject having just entered the space when the event starts. The simulated scene is a room with the dimensions of 4.7 m length × 4.4 m width × 2.7 m height. As shown in Figure 1, two computational thermal manikins (CTMs) are placed in a face-to-face position, where manikin A in red represents the infected subject and manikin B in purple refers to the susceptible one. Each manikin shares the same geometry of an average-sized woman, with a height of 1.67 m, standing on the central plane of the room. The periodic sinusoidal breathing is maintained for the manikins during the simulation. The room is in 6 air changes per hour (ACH) and the air temperature is controlled at 24 °C, which is the common room air temperature in an air-conditioned room. Mixing ventilation is adopted, with the air supply opening ($Ø_{d1}$ = 0.4 m) in the middle and the exhaust diffuser (0.1 m × 0.2 m) in the corner of the ceiling. The experimental studies focusing on short-term events were conducted in a full-scale test room with three ventilation types. Two

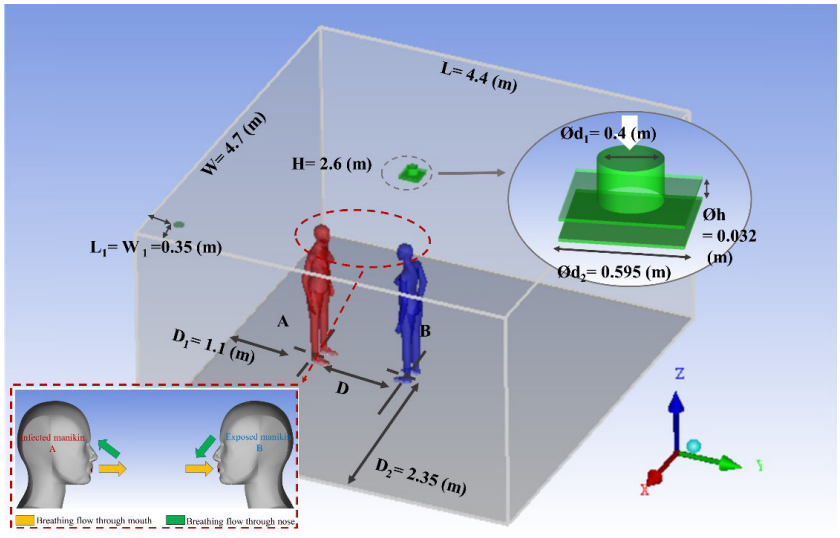

Fig. 1 Simulation scenario with mixing ventilation, the physical distance (D) is adjusted by moving the position of the susceptible subject (B)

breathing thermal manikins were placed in the chamber with different standing positions and physical distances. The tracer gas concentration was monitored by the instruments, including a Fast Concentration Meter and an INNOVA Multi-gas Sampler and Monitor, to evaluate the transient exposure indices. The experimental study examined the dynamic characteristics of short-term events, and a detailed description of the apparatus and experimental procedures could be found in the previous article (Ai et al. 2019a). The boundary effect raised from the room walls in the domain would not influence the human micro-environment.

In order to further reveal the mechanism of the airborne transmission, the separation of the transmission routes (namely, the direct and indirect ways), is conducted. The additional experiments are performed in a large space (with nearly 2870 m^3) that is a university canteen at off-time, where a human subject simulates an infected person and the CO_2 concentration in the breathing zone of a thermal manikin placed in front of the subject is monitored. It is believed that the exhaled CO_2 from a single subject is rapidly diluted into the indoor air of a large space and the building-up of the CO_2 concentration in the background (referring to indirect exposure) is negligible, especially during short-term events. Under this circumstance, the airborne transmission between the subject and the manikin should include only direct exposure.

Since the interaction between the thermal convective boundary layer, respiratory flow, and ventilation flow largely determines the relative role of direct and indirect airborne transmission, three physical distances (D), namely 0.35 m, 1.0 m, and 1.5 m, are employed to analyze the threshold between direct and indirect transmission in short-term events. The concentration of inhaled contaminants is monitored through the sampling point in the center of the lips. In addition, the relative orientation between the two subjects is a critical factor affecting the risk of airborne transmission in a short distance. The present study considers only the face-to-face orientation, as it is the riskiest arrangement under mixing ventilation (Ai et al. 2019b).

3.2 Boundary conditions

It has been reported that the skin temperature of the human body segments is different, and the difference might be greater than 3 °C (Zaproudina et al. 2008). In addition, the temperature difference among the human skin and clothing is notable owing to the insulation characteristics of the clothing (Licina et al. 2014). To accurately reproduce the thermal convective boundary layer around the body, the CTM is divided into seven regions (as shown in Figure 2) and different skin temperatures are defined. The total heat power of each manikin is defined to be 80 W (Ai et al. 2019a), where the convective heat load accounts for approximately 30%. Since the present study mainly focuses on the unsteady-state flow field and contaminant distribution between two human subjects in short-term events, the surrounding regions of the human body are refined by a smaller expansion ratio. The global refinement of the entire mesh is not necessary, especially for the region on the manikin's right side at the physical separation distance of 0.35 m (in Figure 2(a)). While the physical distance increases to 1.0 m and 1.5 m, the aforementioned region in a high aspect ratio will disappear.

As for the breathing mode, the infected subject is inhaled by the nose and exhaled by the mouth, while the

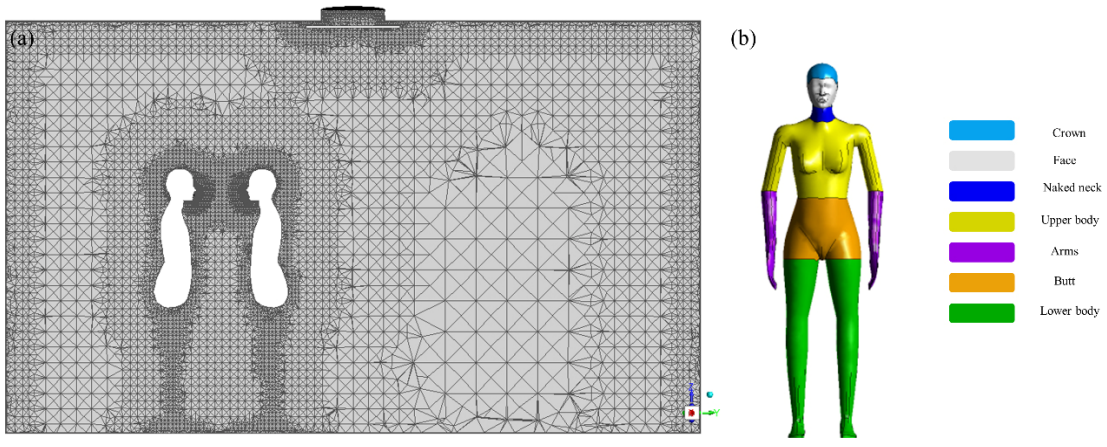

Fig. 2 (a) the grid arrangement in the domain; (b) the division of the computational thermal manikin for segmental skin variation

susceptible subject is inhaled by the mouth and exhaled by the nose. The above combination has been recognized as the worst breathing condition in terms of the risk of cross-transmission (Villafruela et al. 2016). The cross-sectional area of each nostril is 38.5 mm^2, and that of the mouth is 158 mm^2 (Melikov 2004). The two jets from the nostrils are inclined 45° downwards from the horizontal plane and 30° from each other (Xu et al. 2017), and the flow from the mouth is roughly horizontal. The pulmonary ventilation rate and respiratory rates are 6.0 L/min and 10 times/min, respectively. Respiratory activities of the CTMs follow the sinusoidal function and each breathing cycle is composed of inhalation (2.5 seconds), exhalation (2.5 seconds), and break (1.0 seconds) (Bolashikov et al. 2015; Yang et al. 2015). The mass fraction of tracer gas (N_2O) in the exhalation air of the infected subject is 0.027 (Ai et al. 2020). The user-defined function is employed to add the respiratory equations to the mouth and nostrils boundary condition, and therefore the breathing speed change would follow the sinusoidal curve, as shown in Figure 3. The other boundary conditions are presented in Table 1.

The Pressure Implicit with Split Operator algorithm (PISO) is adopted to solve the flow field. As for the space discretization of the energy, momentum, and density, the second-order upwind scheme is employed. The transient

Table 1 the setting of numerical boundary conditions

Boundary	Setting
Mouth area	158 mm^2
Nostril area	77 mm^2
Breathing rate	6.0 L/min
Breathing frequency	10 times/min
Breathing velocity	User-defined function
Air inlet	V=0.74 m/s
Air outlet	Pressure outlet
Room wall	Adiabatic
Human body	Different temperature
Mass fraction of tracer gas	0.027

formulation is resolved by the second-order implicit method. The time step is defined as 0.04 s. Large-eddy turnover time is the characteristic timescale defined as the largest scale of the computational domain (w) divided by the friction velocity (v_0). In this study, the w = 4.7 m, and estimated v_0 could be obtained by dividing the ventilation flow rate by a half section of the domain. The convergence test would be performed by evaluating the variability of the time-averaged values with a 5 eddy turnover time, and 5 eddy turnover time has been larger than that proposed by Villafruela et al. (2016).

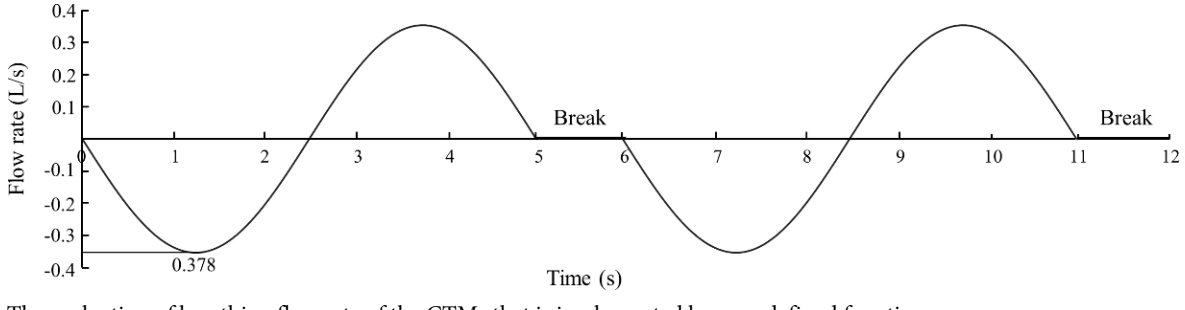

Fig. 3 The evaluation of breathing flow rate of the CTMs that is implemented by user-defined function

3.3 Grid independence test and model validation

To save the computational cost and guarantee the reliability of the simulation, the grid independence test is carried out before the simulation. Owing to the complex human body geometry, tetrahedral cells have been employed to accurately fit the realistic geometry. The finest cell size is kept around 0.0008 m at each manikin's mouth and nose, and the cell of the face gradually expands up to 10 times. The maximum cell size of the face is maintained within 10 times of that at the mouth (Villafruela et al. 2013), and the maximum cell size of the body was maintained within 4 times of the maximum cell size of the face. As a result, each CTM has approximately 80000 triangles on its surface. At the same time, five layers of prismatic cells are generated by extruding the surface triangles away from the surface to ensure that the $y+$ is less than 1. In this way, the grid could ensure a good resolution in the boundary layer, providing the best support for LES.

Three sets of grid distribution are tested, including fine: 5.7 million, medium: 3.4 million, and coarse: 1.8 million. The velocity results along the sampling line above the manikin (see Figure 4(a)) are employed to examine the gird independence, and the comparison of the results given by using the three grids is shown in Figure 4(b). The medium and fine grids provide quite similar results, and the difference in the dimensionless velocity given by the fine and medium grids is 3.7%. In addition, the medium grid with 3.4 million cells is able to refine the surrounding regions of human bodies. The skewness of more than 99.6% of the cells is less than 0.91 (Ansys 2009). Therefore, the simulations are conducted with the medium grid to save computational time.

The model validation based on the surrounding flow field around the CTM has been performed. The simulation results are compared to the particle image velocimetry (PIV) measurements at the ambient air temperature of 20 °C (Licina et al. 2014). In addition to the LES model, the RNG k–ε model is also employed to do the comparison, by keeping the same settings with the LES model. Flow speeds at fifteen points at different heights in front of the thermal manikin are measured. The simulation results from 61 s to 65 s at each point are averaged and compared with the experimental data, as presented in Figure 5. In general, the simulation results agree well with the experimental data at most points, though relatively large discrepancies occur in the region in front of the face. The reasons could be firstly the imperfection of the numerical model and settings and secondly the limitation of the measurements in terms of the inaccurate determination of the sampling location and the intrusion of the sampling tube. In comparison with the LES model, the unsteady RANS approach just models the turbulence and resolves only unsteady mean flow structures (Arpino et al. 2022). Since the present study focuses on short-term events, the contaminant fluctuation depends not only on the turbulence intensity near the facial region, but it could also be affected by the turbulent energy distribution among the eddies of different sizes. Therefore, it is of critical importance to employ the LES turbulence model to resolve the eddies of the turbulence itself.

4 Results and analysis

4.1 Interaction of flows in breathing zone

Figure 6 presents the contours of the mass fraction of N_2O on the central plane of the chamber. In the physical distance of 0.35 m, as shown in Figure 6(a), the high contaminant concentration is observed in the breathing zone of the susceptible subject. Owing to the high momentum of respiratory flow, the exhaled aerosols surrogated by tracer gas could penetrate the thermal convective boundary layer

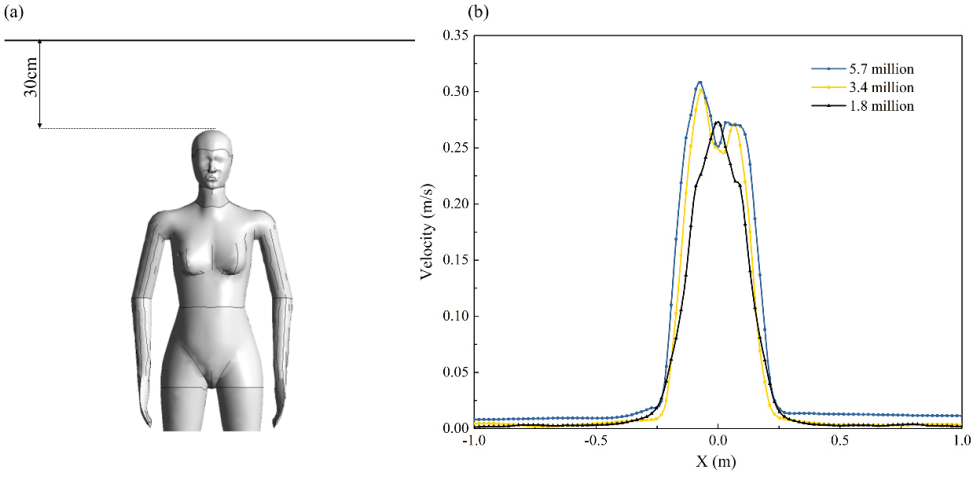

Fig. 4 Grid independence test: (a) the location of sampling line; (b) the comparison of the velocity results

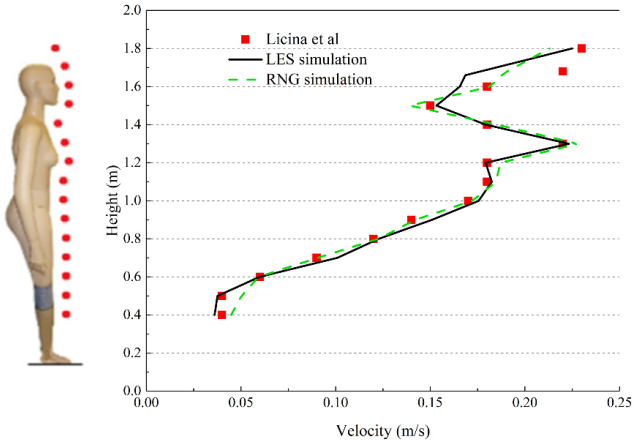

Fig. 5 Comparison of velocity results given by the simulation and the experiment (Licina et al. 2014)

and the exhaled flow of the susceptible subject at this close physical distance. In addition, the nose exhalation (namely, the susceptible subject) is less effective in removing the contaminants in the breathing zone. However, at the physical distance of 1.0 m and 1.5 m (Figures 6(b) and (c)), it is rather difficult for the exhaled flows to penetrate the thermal convective boundary layer. Exhaled contaminants would move upward and cross over the susceptible subject under the effect of thermal convective boundary layer, diluting into the indoor air. In all distances, the phenomenon of backward movement of exhaled flows to the upper region of the infected subject is observed, thus increasing the contaminant concentration close to the infected subject's face. This phenomenon is also reported in a previous study based on dynamic breathing condition (Villafruela et al. 2013). In theory, direct airborne transmission refers to the direct inhalation of exhaled contaminant owing to the close contact, and indirect transmission represents sharing of the background concentration. Given that the exposure concentration decreases considerably when the distance increases from 0.35 m to 1.0 or 1.5 m, the direct and indirect airborne transmission could be identified in the range from 1.0 to 1.5 m, which is consistent with other studies (Liu et al. 2017; Liu et al. 2019).

Further analysis of the transient interaction of the ventilation flow, respiratory flow, and thermal convective boundary layer around the two CTMs is made. Figure 7 presents the velocity vector fields at two different moments

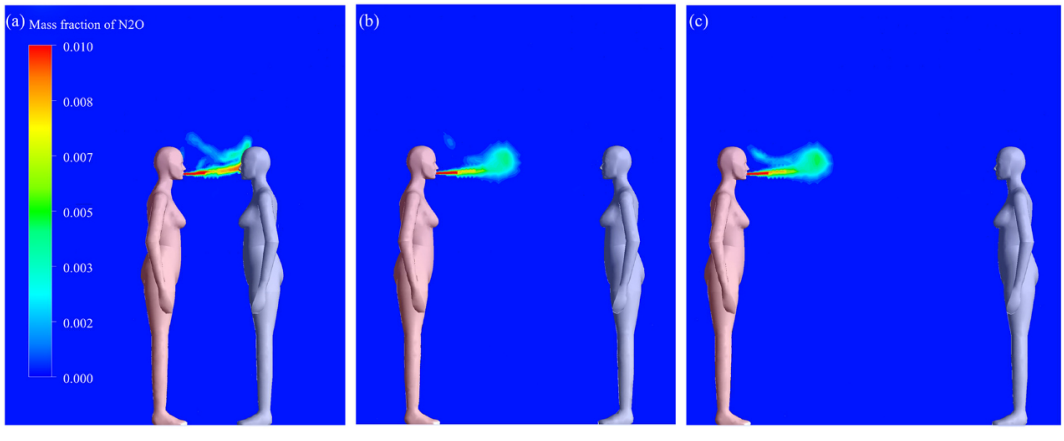

Fig. 6 The mass fraction of N_2O on the central plane of the chamber with different physical distances: (a) D = 0.35 m; (b) D = 1.0 m; (c) D = 1.5 m. CTM in red represents the infected subject and CTM in purple refers to the susceptible one

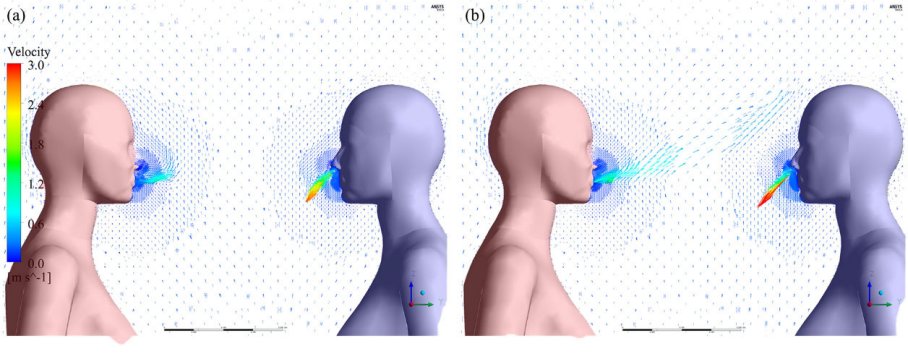

Fig. 7 Transient velocity vector field in the breathing zone of the two manikins at the physical distance of 0.35 m: (a) 0.5 s after the start of the exhalation phase; (b) 1.5 s after the start of the exhalation phase. CTM in red represents the infected subject and CTM in purple refers to the susceptible one

in the exhalation process during the 20th calculated breathing cycle. When the flow is exhaled from the mouth of the infected subject, it moves upward at a distance of 0.075 m away from the mouth. A large-scale vortex is formed on the top side of the mushroom-shaped flow. The mouth breathing flow is strongly affected by the thermal convective boundary layer, which is demonstrated in some previous experiments and simulations (Feng et al. 2015; Feng et al. 2020). In comparison, the influence of the thermal convective boundary layer on the flow jets from the nostrils is insignificant, as the exhaled flow from nostrils has a relatively high speed and a certain downward inclination angle. When losing the initial momentum, the flow jets exhaled from the nostrils would be dragged upwards under the effect of buoyancy. However, the existence of a high-speed exhaled flow from the nostrils of the susceptible subjects could promote the generation of a low-pressure recirculation in front of the face, which might further leads to the entrainment of surrounding air (including that exhaled by the infected subject) into the breathing zone (Ai and Melikov 2018). At a later stage of the exhalation process (see Figure 7(b)), the exhaled flow could directly penetrate into the breathing zone of the susceptible subject and causes risk.

4.2 Comparison of short-term and steady-state exposure

As aforementioned, the short-term exposure events could be different depending on the status of the indoor background concentration, namely, the steady-state condition and the building-up condition (Ai et al. 2019c). For the building-up condition, the exposure characteristics could be distinctive if the exposure duration is different. Figure 8 presents the comparison of the exposure index of various short-term events and steady-state event (30 min) based on two exposure indices, namely the time-averaged and phase averaged one. Phase-averaged exposure index is calculated only from contaminant concentration sampled in the inhalation phase. In comparison, time-averaged exposure index is calculated from the arithmetic mean contaminant concentration continuously in the exposure event. The error bars refer to the standard deviations of the aforementioned two exposure indices. As shown in Figures 8 (a)(b)(c), the significant standard deviation of exposure indices is found at a separation distance of 0.35 m during short-term events, which is more moderate at a distance of 1.0 m and 1.5 m. The large fluctuations demonstrate the randomness and discreteness characteristics of short-term events (detailed analysis in Section 5). In theory, when the ambient air is completely mixing under steady-state condition, the exposure index should be unity (1.0). In the present study, the exposure index slightly deviates from the unity (1.0) due to the intermittent exhalation of the contaminant and the high-turbulent characteristics of the flow in the breathing zone.

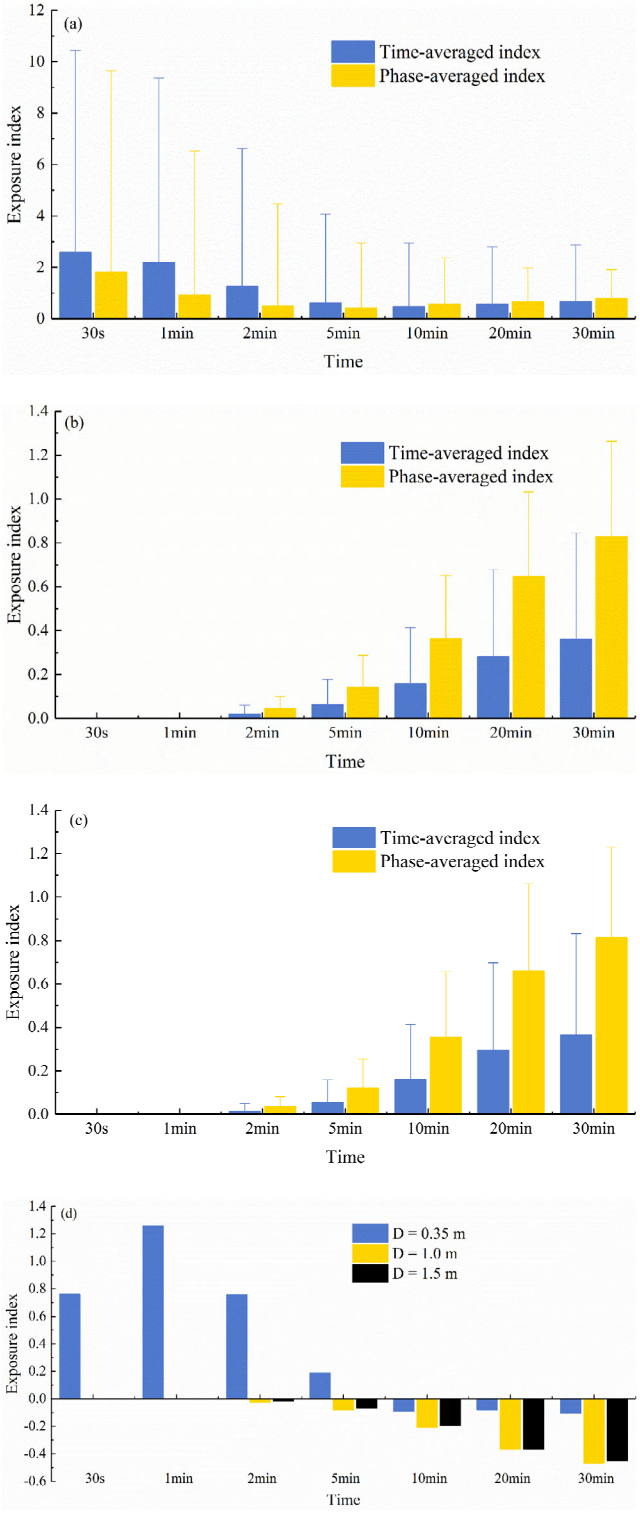

Fig. 8 Variation of the time-averaged and phase-averaged exposure indices during short-term events under different conditions: (a) physical distance of 0.35 m; (b) physical distance of 1.0 m; (c) physical distance of 1.5 m; and (d) the difference between the time-averaged and phase-averaged exposure indices

In Figure 8(a), the physical distance between the two subjects is 0.35 m, and the largest time-averaged and phase-averaged exposure indices occur in the event duration of 30 s, which are approximately 3 times larger than that under the steady-state condition (30 min). The exposure index does not consistently increase over time, especially before 10 minutes, which agree with previous experimental studies (Ai et al. 2019a). The high fluctuation characteristics of the inhaled contaminant concentration could be accounted for by the strong flow interaction in the breathing zone. The large difference between the time-averaged and phase-averaged exposure indices is observed at the initial stage, and the difference becomes smaller with the increase of event duration. The phenomenon is caused by the absence of phase difference between two breathing cycles, and the high contaminant concentration presented in the breathing zone of the susceptible subject is in the exhalation phase (infected subject mouth exhalation and susceptible one nose exhalation). As shown in Figures 8(b) and (c), the time and phase averaged exposure indices of susceptible subjects at distances of 1.0 m and 1.5 m are generally in the same trend, and both are obviously lower than that at the distance of 0.35 m. Since the exhaled pollutants cannot penetrate the thermal convective boundary layer of the susceptible subject at the distances of 1.0 m and 1.5 m, the time-averaged and phase-averaged exposure indices are very low in the short-term events within 2 minutes-duration. As the background concentration of contaminants gradually increases, with the increase of event duration, the exposure index also increases. The difference between the time-averaged and phase-averaged exposure indices in the long physical distance is owing to the form of negative pressure zone in the mouth-inhalation phase, allowing the background contaminant to enter the breathing zone of the susceptible subjects. Figure 8(d) refers to the relative difference between the time-averaged and phase-averaged exposure indices at three physical distances, where the positive value refers to that the time-averaged exposure index is larger than the phase-averaged one. It indicates the relative magnitude of the difference of two exposure indices except for their standard deviations. Due to the clear difference between indices with different trends, both time-averaged and phase-averaged exposure indices are required to be evaluated in the short-term events.

4.3 Comparison of exposure index under short and long distances

The relationship between the physical distance and the phase-averaged exposure index for short-term events with different durations is presented in Figure 9. Firstly, the physical distance still acts as a critical parameter for airborne transmission, which refers to the phase-averaged exposure index generally decreasing as the increase of physical distance. At a close distance, the exhaled contaminant could directly penetrate the thermal convective boundary layer of the susceptible subjects. The susceptible subject is directly exposed to the infected individual. When the physical distance increases to 1.0 m or 1.5 m, the phase-averaged exposure index could decrease. The increasing trend and small fluctuation characteristics at a separation distance of 1.0 m are generally in line with those of 1.5 m. This may suggest that the indirect transmission dominates the airborne transmission route, when the physical distance is larger than 1.0 m. Secondly, the phase-averaged exposure index may not consistently decline as the physical distance increases. As shown in Figure 9, the index ($\varepsilon_{0.35m}$ = 0.651) first slightly declines ($\varepsilon_{1.0m}$ = 0.647) and then goes up ($\varepsilon_{1.5m}$ = 0.659) with the distance for the exposure period of 20 minutes. The phenomenon could be accounted for by the instability characteristics of the direct airborne transmission, and it always occurs at a close physical distance. The detailed assessment of the characteristics of the direct airborne route would be analyzed in Section 4.4. Thirdly, the phase-averaged exposure index does not consistently go up over time, particularly for a short physical distance. Before the 10 min time threshold, the phase-averaged exposure index at 0.35 m slightly decreases over time. After this time threshold, the index slowly increases over time owing to the increasing background concentration and the occurrence of the indirect airborne transmission route. It appears that the direct airborne transmission route plays a more critical role than the indirect one at a short separation distance during short-term events. Owing to the presence of direct and indirect airborne transmission in the short separation distance, the change of the room ventilation rate could affect the time threshold and the occurrence time of the indirect airborne route. In order to further understand

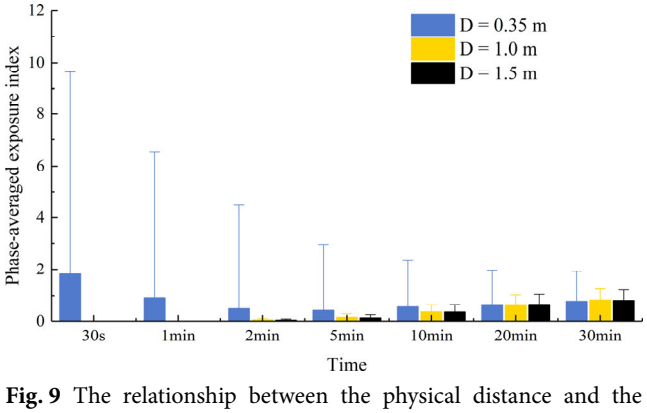

Fig. 9 The relationship between the physical distance and the phase-averaged exposure index in short-term events with different durations

the mechanism of airborne transmission, it is important to separate the direct and indirect airborne transmission routes.

4.4 Separation of the airborne transmission routes

Notably, the employed time-averaged and phase-averaged exposure index (as presented in Figures 8 and 9) just indicate the average contaminant concentration inhaled by the susceptible subject, but do not reveal the cumulation of inhaled contaminant over time. Figure 10 presents the cumulative exposure index at different physical distances. The cumulative exposure index continues to grow over time, and the physical distance still acts as the dominant role in the exposure assessment. Differences are found in the growth rate of the exposure index between the scenarios at different physical distances and with different exposure durations. The exposure risk in a 2-minute exposure event at the distance of 0.35 m is approximately equal to that in the 12-minute exposure scenario at 1.5 m/1.0 m. In addition, at the distance of 0.35 m, the difference between the slopes before and after 10 min may be due to the change in the relative role of the two airborne transmission routes, namely direct or indirect transmission. The insight of the characteristics of airborne transmission could help to develop accurate mitigation measures.

According to the occurrence time of the indirect airborne transmission route in this study, it is assumed that indirect exposure could increase uniformly after 10 minutes. As mentioned above, the two airborne transmission routes occur when the susceptible subject is in close proximity to the infected one (at 0.35 m), and only the indirect route exists at large physical distances (at 1.0 m/1.5 m). In this way, the direct exposure of airborne transmission at a distance of 0.35 m can be calculated by subtracting the exposure at 1.5 m (representing indirect exposure) from the exposure at 0.35 m (representing total exposure). The results of experiments performed in the large-space university canteen (see Section 3.1 for details) are also used for comparison. As presented in Figure 11, the direct exposure indices at different physical distances are compared through the normalization $\overline{\varepsilon_i(m)} / \sum \overline{\varepsilon_i(m)}$ where $\overline{\varepsilon_i(m)}$ refers to the direct exposure indices for the interval of time m. In Figure 11(a), the direct exposure indices obtained by simulation and experiment have presented the same instability characteristics. In comparison with the indirect exposure index stably increasing with time, the direct exposure index could fluctuate over time. The instability might be accounted for by the presence of turbulence, rising from the strong flow interaction in breathing zone. In addition, the percentage of direct exposure to total exposure could also change largely over time, and it fluctuates around 40% after 10 minutes. Note that this percentage should be strongly influenced by the air change rate of the space. Figure 11(b) presents the direct exposure indices in the supplementary experiment study with three close physical distances (0.25 m, 0.35 m, and 0.5 m). Since the background concentration (referring to indirect exposure) in the large experimental space is negligible, the averaged direct exposure indices obtained in the three close distances would be presented as generally similar. Nevertheless, the discreteness of the exposure index generally decreases with increasing physical distance. Considering the randomness,

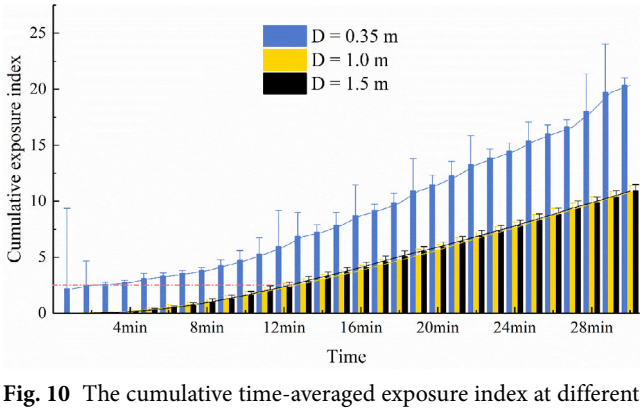

Fig. 10 The cumulative time-averaged exposure index at different physical distances with the interval of 1 min

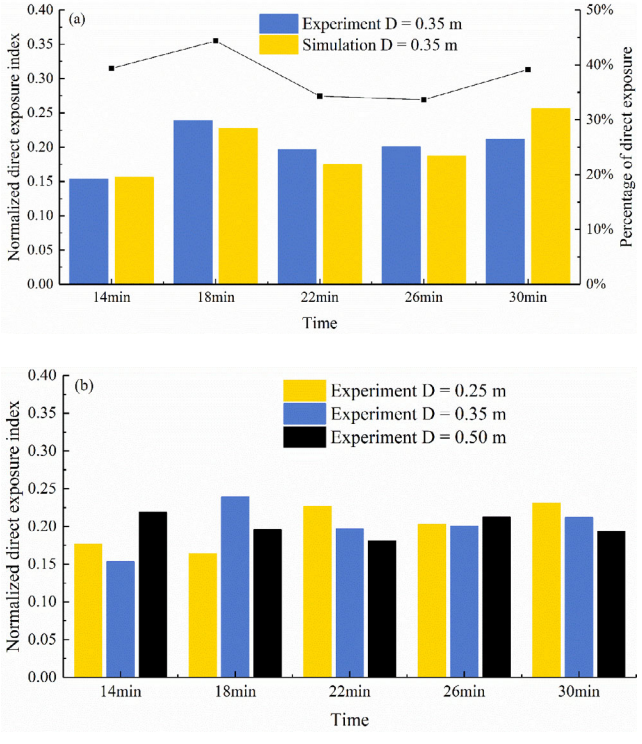

Fig. 11 Comparison about the normalized direct exposure indices at different physical distances: (a) the results obtained by simulation and experiment at a distance of 0.35 m; (b) the direct exposure indices at three close distances

discreteness, localization, and high-risk characteristics of direct airborne transmission route, current precautionary actions and the dilution ventilation aiming for the whole space under steady-state condition could not be high-efficient for the short-term events.

5 Discussion

Depending on the exposure duration and separation distance, airborne transmission could be divided into two categories and four combinations, namely, (a) steady-state exposure: short-distance and long-distance; (b) short-term exposure: short-distance and long-distance. Many previous studies focused on steady-state exposure (Bhattacharyya et al. 2020; Srivastava et al. 2021; Motamedi et al. 2022), but fewer studied the short-term exposure events. In real life, there are many short-term exposure events, such as the consultation of physicians, short meetings, offices, classrooms, canteens, etc. In response to the Delta and Omicron variants of SARS-CoV-2, the airborne transmission in the short-term events should be well recognized by the public health authorities. Maintaining physical distance and wearing masks continue to be effective mitigation strategies for the Delta and Omicron variants (Khosronejad et al. 2020; Leonard et al. 2020). To maintain the health and well-being of urban dwellers (Li et al. 2019), the physical distancing is still recommended for short-term events.

In contrary to the previous study (Nielsen et al. 2008), the result of this study illustrates that the exposure index for the short-term exposure events might not consistently increase over time until reaching the steady-state condition. During the short-term events with a short physical distance (0.35 m), the largest time-averaged exposure index is presented in the short-term events with the duration of 30 s, where the exposure index is around 3 times higher than that of the steady-state condition. As mentioned early, the short-term events investigated in the present study is restricted to the scenarios with building-up background concentration. The strong interaction of flows in the breathing zone could result in the inhaled concentration being unstable and changing over time (Ai et al. 2019a). The magnitude of concentration fluctuation also affects the exposure in short-term events. Therefore, the time or phase averaged exposure index might be smaller in the steady-state condition (as an example shown in Figure 8). The obtained result also explains that the reported infection of the Delta variant of SARS-CoV-2 may occur in tens of seconds (Kongnov 2021). In addition, the exposure index investigated in this study for various short-term events might not consistently decline as the physical distances increase (as presented in Figure 9), the obtained results are not consistent with the observation under steady-state conditions (Bolashikov et al. 2012; Olmedo et al. 2013). Because of the random fluctuation of the direct airborne transmission route during short-term events, the higher value of the time-averaged exposure index could occur in the relatively long physical distance. In general, the difference between the short-term events and the steady-state condition implies that the current mitigation methods and the dilution ventilation based on the steady-state condition might not be high-efficient for the short-term events. The development of effective precautionary measures aiming for short-term or unsteady exposures events is expected to receive much more attention.

The large fluctuation characteristics of the short-term exposure index are observed, no matter in the short and the long physical distance. Owing to the instantaneous and tidal characteristics of the exhalation jet, it becomes fully turbulent and further mixes with the surrounding air with the development of flow. In addition, the interaction between respiratory flow, the ventilation flow, and the thermal convective boundary layer rising from the heated human body increases the turbulence level in the breathing zone of susceptible subjects. For example, at the physical distance of 0.35 m, the high fluctuation of the concentration of contaminants inhaled by the susceptible subjects can be explained by the strong interaction between the flow of two exhalations. The interaction may cause the inhomogeneous distribution of concentration in the breathing zone. Therefore, it is absolutely necessary to distinguish the difference between concentration distribution in the breathing zone and that inhaled by the susceptible subject. At the long physical distance like 1.0 m and 1.5 m, the relative lower fluctuation of the concentration is due to the mixing and dilution effect of the surrounding flow.

The infection risk assessment could act as an effective tool to evaluate the exposure risk of susceptible subjects and validate the performance of the corresponding precautionary measures. In this study, an improved evaluation method proposed by Ai et al. (2019a) is employed to evaluate the airborne transmission risk under the short-term events. The traditionally widely used risk-evaluation methods such as the Wells-Riley equations, IF (intake fraction), and exposure index have presented their limitations with regard to the unsteady and short-term exposure events. Considering that there are many short-term events in practice and that even the steady-state and complete-mixing are not reached before the end of the events, the improved evaluation method makes it possible to evaluate both real-time exposure risk of the susceptible subject at one particular moment and time-averaged exposure risk over a given period.

Increasing the room ventilation rate is a widely recommended measure to dilute the concentration and further control the airborne transmission. However, the direct

airborne transmission occurs with the direct exposure of the virus-laden droplets and aerosols when the subjects are in close physical proximity. The results of the present study illustrate that direct airborne transmission is much more important than indirect one in short-term events. This is because the room ventilation could dilute and reduce the background concentration, but the background value in the short-term events is relatively lower and not uniform than that in the steady state. Therefore, the general dilution ventilation has a limited impact on the direct airborne transmission in short-term events. In addition, the separation of the airborne routes and the further assessment of their associated properties have proven the previous hypothesis that the SARS-CoV-2 transmission is predominated by the direct airborne route (Li 2021). Compared to the limited impact on the direct airborne route, the general dilution ventilation could determine the occurrence time of indirect one. The relationship between different room ventilation rates and the occurrence time of indirect airborne route needs further assessment. Owing to the randomness, discreteness, localization, and high-risk characteristics of the direct airborne route, the current precautionary actions and the dilution ventilation based on the whole space under steady-state condition could not be high-efficient for the short-term events. The localized ventilation/exhaust system, air curtain, physical barrier, and air filtration should be highly recommended. From the perspective of engineering control, protection measures can be divided into two types, namely, control of the emission from the infected and protection of the susceptible. The widely recommended surgical mask may help to filter most of droplets and also extinguish the exhalation jet. A physical barrier would also be effective to block the exhalation jet (Ye et al. 2021). For places with a high requirement, the escaping fine particles could be further removed by a localized exhaust system.

As for the limitation of this study, the exhaled contaminant is surrogated by the tracer gas. The discrete phase with evaporation process is not considered for several reasons: Firstly, the size distribution of the respiratory droplet and aerosol particles are found in the range from 0.25 to 40 μm, and the most fall into the 1–4 μm (Ai et al. 2020). Given that the main driving force for the respiratory particles in the indoor environment is the airflow rather than the gravity (Nazaroff 2016), the tracer gas is suitable to simulate this commonest range of respiratory particles (Ai et al. 2020). Secondly, the evaporation process is instantaneous for small droplets (Holmgren et al. 2011). A 3 and 5 μm pure-water droplet would evaporate at 97% relative humidity in less than 0.33 s and 0.8 s, respectively (Morawska et al. 2009). Therefore, the present study employs the tracer gas rather than the discrete phases with evaporation to simulate the transmission of the respiratory particles. Future study should examine the transmission pattern of the large droplets. In addition, the study is limited to the condition where human is still, while the movement of the body significantly affects the convective boundary layer and further influences the cross-transmission (Cao et al. 2017). The present study does not consider the droplet route and surface contact route, which, however, contribute a lot to the overall risk of cross infection. Finally, it should be noted that the study only focuses on the scenario of building-up background concentration at a certain air change rate (namely, 6 h^{-1}).

6 Conclusions

The present study on direct and indirect airborne transmission during short-term events allows the following conclusions to be drawn:

1) The exposure index in the short-term events varies largely over time, especially within the first 1/ACH hour (namely, 10 minutes in the present study) of exposure between occupants in close proximity. Due to such a considerable variation, there is a high uncertainty related to the spatial and temporal evolutions of the risk of cross infection.
2) The decoupling and analysis of the direct and indirect airborne transmission routes have shown that the direct airborne transmission acts as the predominated route in short-term events. The conventional dilution ventilation has a limited influence on the direct airborne transmission route, but, to a large extent, determines the occurrence time of indirect one.
3) Owing to the randomness, discreteness, localization, and high-risk characteristics of direct airborne transmission, the current precautionary measures aiming for the whole space under steady-state conditions are not high-efficient to the short-term events, and localized methods like localized ventilation/exhaust system and physical barrier that can effectively destroy the direct airborne transmission route should be more effective and less costly.

Acknowledgements

This study was supported by the National Natural Science Foundation of China (No. 51908203) and by the Fundamental Research Funds for the Central Universities (No. 531118010378). The authors thank Miss Zenan Xian for her help throughout this study.

Declaration of competing interest

The authors have no competing interests to declare that are relevant to the content of this article.

Author contribution statement

All authors contributed to the study conception and design. Material preparation, data collection and analysis were performed by Xiujie Li, Zhengtao Ai, and Jinjun Ye. The first draft of the manuscript was written by Xiujie Li, and Zhengtao Ai. All authors commented on previous versions of the manuscript. All authors read and approved the final manuscript.

References

Ai Z, Mak CM, Niu J (2013). Numerical investigation of wind-induced airflow and interunit dispersion characteristics in multistory residential buildings. *Indoor Air*, 23: 417–429.

Ai Z, Mak CM (2014). A study of interunit dispersion around multistory buildings with single-sided ventilation under different wind directions. *Atmospheric Environment*, 88: 1–13.

Ai Z, Mak CM (2015). Large-eddy Simulation of flow and dispersion around an isolated building: Analysis of influencing factors. *Computers and Fluids*, 118: 89–100.

Ai Z, Melikov AK (2018). Airborne spread of expiratory droplet nuclei between the occupants of indoor environments: A review. *Indoor Air*, 28: 500–524.

Ai Z, Hashimoto K, Melikov AK (2019a). Airborne transmission between room occupants during short-term events: Measurement and evaluation. *Indoor Air*, 29: 563–576.

Ai Z, Hashimoto K, Melikov AK (2019b). Influence of pulmonary ventilation rate and breathing cycle period on the risk of cross-infection. *Indoor Air*, 29: 993–1004.

Ai Z, Huang T, Melikov AK (2019c). Airborne transmission of exhaled droplet nuclei between occupants in a room with horizontal air distribution. *Building and Environment*, 163: 106328.

Ai Z, Mak CM, Gao N, et al. (2020). Tracer gas is a suitable surrogate of exhaled droplet nuclei for studying airborne transmission in the built environment. *Building Simulation*, 13: 489–496.

Ansys (2009). ANSYS Fluent 12.0 User's Guide. Ansys Inc.

Armand P, Tâche J (2022). 3D modelling and simulation of the dispersion of droplets and drops carrying the SARS-CoV-2 virus in a railway transport coach. *Scientific Reports*, 12: 4025.

Arpino F, Cortellessa G, Grossi G, et al. (2022). A Eulerian-Lagrangian approach for the non-isothermal and transient CFD analysis of the aerosol airborne dispersion in a car cabin. *Building and Environment*, 209: 108648.

Bhatia D, De Santis A (2020). A preliminary numerical investigation of airborne droplet dispersion in aircraft cabins. *Open Journal of Fluid Dynamics*, 10: 198–207.

Bhattacharyya S, Dey K, Paul AR, et al. (2020). A novel CFD analysis to minimize the spread of COVID-19 virus in hospital isolation room. *Chaos, Solitons & Fractals*, 139: 110294.

Bolashikov ZD, Barova M, Melikov AK (2015). Wearable personal exhaust ventilation: Improved indoor air quality and reduced exposure to air exhaled from a sick doctor. *Science and Technology for the Built Environment*, 21: 1117–1125.

Bolashikov ZD, Melikov AK, Kierat W, et al. (2012). Exposure of health care workers and occupants to coughed airborne pathogens in a double-bed hospital patient room with overhead mixing ventilation. *HVAC&R Research*, 18: 602–615.

Cao S-J, Cen D, Zhang W, et al. (2017). Study on the impacts of human walking on indoor particles dispersion using momentum theory method. *Building and Environment*, 126: 195–206.

Dai Y, Mak CM, Ai Z, et al. (2018). Evaluation of computational and physical parameters influencing CFD simulations of pollutant dispersion in building arrays. *Building and environment*, 137: 90–107.

Dai Y, Mak CM, Ai Z (2019). Computational fluid dynamics simulation of wind-driven inter-unit dispersion around multi-storey buildings: Upstream building effect. *Indoor and Built Environment*, 28: 217–234.

Desai PS, Sawant N, Keene A (2021). On COVID-19-safety ranking of seats in intercontinental commercial aircrafts: a preliminary multiphysics computational perspective. *Building Simulation*, 14: 1585–1596.

Du Y, Blocken B, Abbasi S, et al. (2021). Efficient and high-resolution simulation of pollutant dispersion in complex urban environments by island-based recurrence CFD. *Environmental Modelling and Software*, 145: 105172.

Feng L, Yao S, Sun H, et al. (2015). TR-PIV measurement of exhaled flow using a breathing thermal manikin. *Building and Environment*, 94: 683–693.

Feng G, Bi Y, Zhang Y, et al. (2020). Study on the motion law of aerosols produced by human respiration under the action of thermal plume of different intensities. *Sustainable Cities and Society*, 54: 101935.

Gao N, Niu J (2007). Modeling particle dispersion and deposition in indoor environments. *Atmospheric Environment*, 41: 3862–3876.

Hinze J (1967). Secondary currents in wall turbulence. *Physics of Fluids*, 10: S122–S125.

Holmgren H, Bake B, Olin AC, et al. (2011). Relation between humidity and size of exhaled particles. *Journal of Aerosol Medicine and Pulmonary Drug Delivery*, 24: 253–260.

Khosronejad A, Santoni C, Flora K, et al. (2020). Fluid dynamics simulations show that facial masks can suppress the spread of COVID-19 in indoor environments. *AIP Advances*, 10: 125109.

Kongnov T (2021). Delta can spread in 15 seconds. Available at https://www.khmertimeskh.com/50902050/delta-can-spread-in-15-seconds/.

Leonard S, Strasser W, Whittle JS, et al. (2020). Reducing aerosol dispersion by high flow therapy in COVID-19: High resolution computational fluid dynamics simulations of particle behavior during high velocity nasal insufflation with a simple surgical mask. *Journal of the American College of Emergency Physicians Open*, 1: 578–591.

Li X, Wei Y, Zhang J, et al. (2019). Design and analysis of an active daylight harvesting system for building. *Renewable Energy*, 139: 670–678.

Li Y (2021). Hypothesis: SARS-CoV-2 transmission is predominated by the short-range airborne route and exacerbated by poor ventilation. *Indoor Air*, 31: 921–925.

Li X, Mak CM, Ma KW, et al. (2021a). Evaluating flow-field and expelled droplets in the mockup dental clinic during the COVID-19 pandemic. *Physics of Fluids*, 33: 047111.

Li X, Mak CM, Ma KW, et al. (2021b). How the high-volume evacuation alters the flow-field and particle removal characteristics in the mock-up dental clinic. *Building and Environment*, 205: 108225.

Li X, Mak CM, Ma KW, et al. (2021c). Restoration of dental services after COVID-19: The fallow time determination with laser light scattering. *Sustainable Cities and Society*, 74: 103134.

Licina D, Pantelic J, Melikov A, et al. (2014). Experimental investigation of the human convective boundary layer in a quiescent indoor environment. *Building and Environment*, 75: 79–91.

Liu L, Li Y, Nielsen PV, et al. (2017). Short-range airborne transmission of expiratory droplets between two people. *Indoor Air*, 27: 452–462.

Liu F, Zhang C, Qian H, et al. (2019). Direct or indirect exposure of exhaled contaminants in stratified environments using an integral model of an expiratory jet. *Indoor air*, 29: 591–603.

Liu Y, Ning Z, Chen Y, et al. (2020). Aerodynamic analysis of SARS-CoV-2 in two Wuhan hospitals. *Nature*, 582: 557–560.

Liu W, Liu L, Xu C, et al. (2021). Exploring the potentials of personalized ventilation in mitigating airborne infection risk for two closely ranged occupants with different risk assessment models. *Energy and Buildings*, 253: 111531.

Massarotti N, Mauro A, Mohamed S, et al. (2021). Fluid dynamic and thermal comfort analysis in an actual operating room with unidirectional airflow system. *Building Simulation*, 14: 1127–1146.

Melikov A (2004). Breathing thermal manikins for indoor environment assessment: important characteristics and requirements. *European Journal of Applied Physiology*, 92: 710–713.

Melikov AK, Dzhartov V (2013). Advanced air distribution for minimizing airborne cross-infection in aircraft cabins. *HVAC&R Research*, 19: 926–933.

Melikov AK, Ai Z, Markov DG (2020). Intermittent occupancy combined with ventilation: An efficient strategy for the reduction of airborne transmission indoors. *Science of the Total Environment*, 744: 140908.

Morawska L, Johnson GR, Ristovski ZD, et al. (2009). Size distribution and sites of origin of droplets expelled from the human respiratory tract during expiratory activities. *Journal of Aerosol Science*, 40: 256–269.

Motamedi H, Shirzadi M, Tominaga Y, et al. (2022). CFD modeling of airborne pathogen transmission of COVID-19 in confined spaces under different ventilation strategies. *Sustainable Cities and Society*, 76: 103397.

Nazaroff WW (2016). Indoor bioaerosol dynamics. *Indoor Air*, 26: 61–78.

Nielsen PV, Winther FV, Buus M, et al. (2008). Contaminant flow in the microenvironment between people under different ventilation conditions. *ASHRAE Transactions*, 114(2): 632–640.

Olmedo I, Nielsen PV, Ruiz de Adana M, et al. (2013). The risk of airborne cross-infection in a room with vertical low-velocity ventilation. *Indoor Air*, 23: 62–73.

Riley EC, Murphy G, Riley RL (1978). Airborne spread of measles in a suburban elementary school. *American Journal of Epidemiology*, 107: 421–432.

Satheesan MK, Mui KW, Wong LT (2020). A numerical study of ventilation strategies for infection risk mitigation in general inpatient wards. *Building Simulation*, 13: 887–896.

Smagorinsky J (1963). General circulation experiments with the primitive equations: I. The basic experiment. *Monthly Weather Review*, 91: 99–164.

Srivastava S, Zhao X, Manay A, et al. (2021). Effective ventilation and air disinfection system for reducing coronavirus disease 2019 (COVID-19) infection risk in office buildings. *Sustainable Cities and Society*, 75: 103408.

Times K (2021). Delta variant can infect a person within 15 seconds as Cambodia logs 75 total cases of COVID-19 Delta infections. Available at https://www.khmertimeskh.com/50895595/delta-variant-can-infect-a-person-within-15-seconds-as-cambodia-logs-75-cases-of-covid-19-delta-infections/.

Van Doremalen N, Bushmaker T, Morris DH, et al. (2020). Aerosol and surface stability of SARS-CoV-2 as compared with SARS-CoV-1. *New England Journal of Medicine*, 382: 1564–1567.

Villafruela JM, Olmedo I, de Adana MR, et al. (2013). CFD analysis of the human exhalation flow using different boundary conditions and ventilation strategies. *Building and Environment*, 62: 191–200.

Villafruela JM, Olmedo I, San José JF (2016). Influence of human breathing modes on airborne cross infection risk. *Building and Environment*, 106: 340–351.

Wang H, Qian H, Zhou R, et al. (2020). A novel circulated air curtain system to confine the transmission of exhaled contaminants: a numerical and experimental investigation. *Building Simulation*, 13: 1425–1437.

WHO (2022). Weekly epidemiological update on COVID-19. Edition 87, 12 April 2022.

Wu J, Weng W (2021). COVID-19 virus released from larynx might cause a higher exposure dose in indoor environment. *Environmental Research*, 199: 111361.

Xu C, Nielsen PV, Liu L, et al. (2017). Human exhalation characterization with the aid of schlieren imaging technique. *Building and Environment*, 112: 190–199.

Yang J, Sekhar C, Cheong DKW, et al. (2015). A time-based analysis of the personalized exhaust system for airborne infection control in healthcare settings. *Science and Technology for the Built Environment*, 21: 172–178.

Yang C, Yang X, Zhao B (2016). Person to person droplets transmission characteristics in unidirectional ventilated protective isolation room: The impact of initial droplet size. *Building Simulation*, 9: 597–606.

Ye J, Ai Z, Zhang C (2021). A new possible route of airborne transmission caused by the use of a physical partition. *Journal of Building Engineering*, 44: 103420.

Zaproudina N, Varmavuo V, Airaksinen O, et al. (2008). Reproducibility of infrared thermography measurements in healthy individuals. *Physiological Measurement*, 29: 515–524.

Zhang Z, Han T, Yoo KH, et al. (2021). Disease transmission through expiratory aerosols on an urban bus. *Physics of Fluids*, 33: 015116.

Zhao L, Zhou H, Jin Y, et al. (2022). Experimental and numerical investigation of TVOC concentrations and ventilation dilution in enclosed train cabin. *Building Simulation*, 15: 831–844.